Eur. J. Mineral.
2014, **26**, 473–483
Published online February 2014

**Biomineralization and biomimetic materials**

# Nanoprobe crystallographic orientation studies of isolated shield elements of the coccolithophore species *Emiliania huxleyi*

RAMONA HOFFMANN[1,*], ANGELA S. WOCHNIK[2], CHRISTOPH HEINZL[2], SOPHIA B. BETZLER[2], SONJA MATICH[3], ERIKA GRIESSHABER[1], HARTMUT SCHULZ[4], MICHAL KUČERA[5], JEREMY R. YOUNG[6], CHRISTINA SCHEU[2] and WOLFGANG W. SCHMAHL[1]

[1] Department of Earth and Environmental Sciences, LMU, 80333 Munich, Germany
*Corresponding author, e-mail: hoffmann.ramona@lrz.uni-muenchen.de
[2] Department of Chemistry, LMU, 81377 Munich, Germany
[3] Walter-Schottky-Institut, TUM, 85748 Garching, Germany
[4] Department for Geosciences, 72074 Tübingen, Germany
[5] MARUM – Center for Marine Environmental Geosciences, University of Bremen, 28359 Bremen, Germany
[6] Earth Sciences, University College London, London WC1E 6BT, UK

**Abstract:** Coccolithophore algae produce elaborately structured skeletons composed of sub-micrometer-scale calcite crystals. In order to understand calcite crystallization and assembly in a coccosphere with nanoscale resolution, the crystal orientation and interdigitation of the structural units were investigated by transmission electron microscopy imaging, selected-area and nano-probe electron diffraction. Focused ion beam sectioning of coccoliths of the coccolithophore species *Emiliania huxleyi* is used to obtain target-prepared specimens in suitable orientation. We were able to detect and analyze the V-unit, which is overgrown by the R-unit. For the V-unit the [001] direction points perpendicular to the coccolith plane while the [110] axis is tangential to the coccolith ring. The R-unit **c**-axis is parallel and the **b**-axis is perpendicular to the coccolith plane, thus confirming the R- and V-model which was based on scanning electron microscopy and optical microscopy. Furthermore we show that the distal- and the proximal shield element of an individual R-unit of a single segment are tilted by $4° \pm 1°$ with respect to each other. This orientation change is required to obtain the flat domed character of the coccoliths, which is necessary to form the coccosphere. The orientation change between the distal- and the proximal shield element appears continuous.

**Key-words:** Biocrystallization, biomaterials, crystal structure, electron diffraction, TEM, Coccolithophores.

## Introduction

Coccolithophorids are one of the most important groups of primary producers in the oceans (Honjo, 1976). They live in almost all marine habitats and are present from arctic to tropical waters (Winter & Siesser, 1994; Young *et al.*, 1997; 2003). They contribute about 15 % to the global ocean phytoplankton biomass and their calcite exoskeletons are one of the major components of deep sea sediments (Riley *et al.*, 1976). Due to their high abundance in sedimentary rocks (Stanley, 1999) coccolithophorids are of high interest for biostratigraphic dating and paleoclimate studies (McIntyre, 1967; Sato *et al.*, 1991).

Typical coccoliths are formed inside the cell and show a radial structure. The segments of these coccolith rings are characteristically formed by two alternating types of crystal units with sub-vertical crystallographic **c**-axes (V-units) and sub-radial **c**-axes (R-units), respectively (Young *et al.*, 1992, 1999; Young & Henriksen, 2003). The R-unit of *Emiliania huxleyi* consists of distal- and proximal shield elements and a central-area element connected through the inner- and outer tube elements (Fig. 1) (Didymus *et al.*, 1994). Transmission electron microscopy (TEM) and scanning electron microscopy (SEM) investigations showed that in the earliest growth stage of *E. huxleyi* coccoliths, the proto-coccolith ring is an elliptical ring of alternating larger and smaller calcite crystals, which were predicted to also alternate in crystallographic orientation (Young *et al.*, 1992, 1999; Didymus *et al.*, 1994). However, only one of these sets of elements develops during growth of the coccolith, so they constitute almost the entire mature coccolith (Fig. 1d). These units have radial **c**-axes and so are R-units hence the alternate units of the proto-coccolith ring were inferred to be V-units. Although these putative V-units have been imaged by electron microscopy in proto-coccolith rings (Young *et al.*, 1992), their crystallographic orientation has never been determined directly but only inferred by analogy from other coccoliths. Recent studies used the SEM-based electron back-scattered

DOI: 10.1127/0935-1221/2014/0026-2365
0935-1221/14/0026-2365 $ 4.95

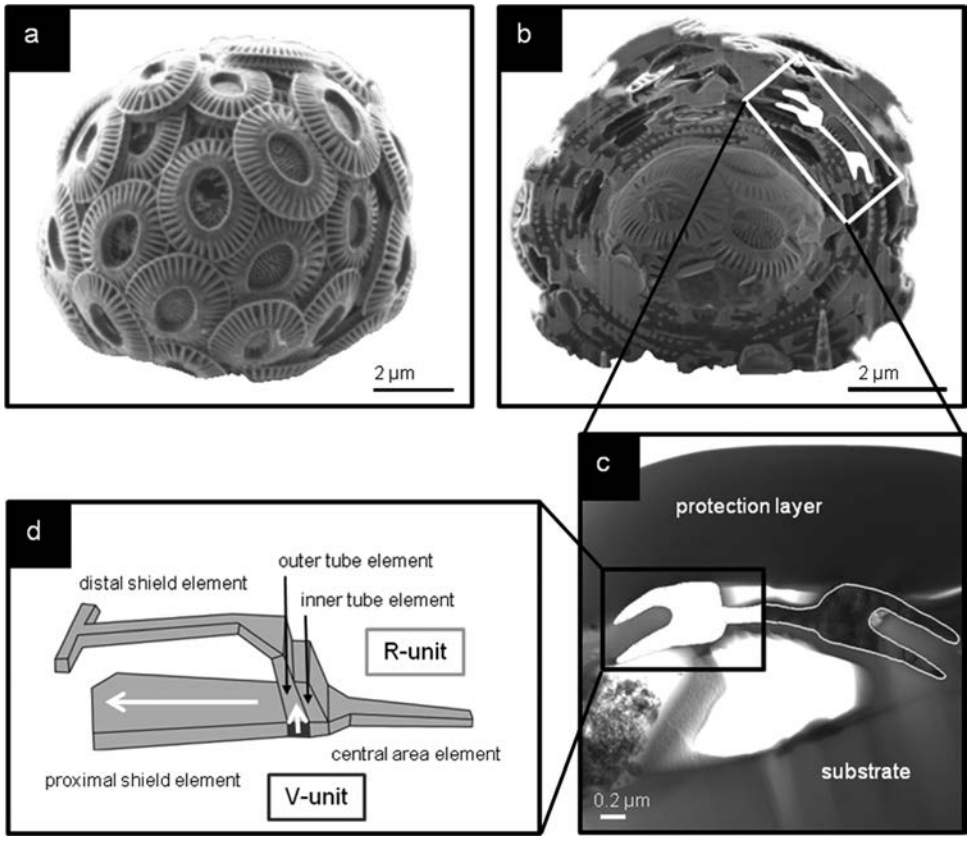


Fig. 1. Calcite skeleton of the marine algae *E. huxleyi*. a) Secondary-electron image of a complete coccosphere of *E. huxleyi*. b) Cross-section obtained by FIB ion-milling through the coccosphere shown in a. The cross-section of a single coccolith is colored white and highlighted by the white frame. c) TEM bright-field image of a cross-section of a single *E. huxleyi* coccolith prepared by FIB sectioning. The coccolith is outlined by a white line. The fully white colored left side of the coccolith cross-section is directly comparable with the schematic model in d). d) Simplified schematic drawing modified from Didymus *et al.* (1994) of one coccolith segment of *E. huxleyi* to visualize the model of Young *et al.* (1992). The R-unit is given in light gray. The longer white arrow pointing parallel to the coccolith plane is indicating the direction of the crystallographic **c**-axis in the R-unit. The V-unit is marked dark gray, with the **c**-axis oriented perpendicular to the coccolith plane (shorter white arrow).

diffraction (EBSD) method (Saruwatari *et al.*, 2006; Saruwatari, 2008a) and Kikuchi pattern orientation in TEM (Saruwatari *et al.*, 2008b) for a more accurate determination of crystal orientations of the R- units of several coccolithophore species (Saruwatari *et al.*, 2006, 2008a and b). Even though the orientation of the crystal units were investigated to some degree in *E. huxleyi* (Wilbur & Watabe, 1963; Watabe, 1967; Mann & Sparks, 1988; Young *et al.*, 1992; Young & Henriksen, 2003; Saruwatari *et al.*, 2008a), the exact nature of their nanostructure and nanoscale architecture is not fully understood. This includes the crystallographic orientation of the V-unit element.

Many carbonate-sequestering marine shelled organisms such as sea urchins, corals and mollusks have skeletons that show a mosaic-like crystal assembly (Neff, 1972; Feng *et al.*, 2000; Weiss *et al.*, 2002; Rousseau *et al.*, 2005; Griesshaber *et al.*, 2007; Jacob *et al.*, 2008; Goetz *et al.*, 2009; Benzerara *et al.*, 2011; Addadi *et al.*, 2012; Schmahl *et al.*, 2012; Seto *et al.*, 2012) where the biocarbonate crystals in their shells are constituted of co-oriented crystallites in the mesoscopic size range (1–1000 nm) (Song & Cölfen, 2010). These mesoscale units are often in very good three dimensional orientational register and show a scattering pattern and behavior in polarized light comparable to that observed in single crystals (Song & Cölfen, 2010). Thus, a further focus of our study was to determine whether the segments of *E. huxleyi* consist of calcite crystals with a mosaic-like assembly or of conventional single crystals. To obtain the required spatial resolution information, we applied TEM and associated analytical techniques including selected-area and nano-probe diffraction experiments, bright-field and high-resolution TEM imaging. To facilitate analysis in cross-section, focused ion beam (FIB) sample preparation was used. We used coccolithophore specimens collected from oceanographic samples.

## Materials and methods

### Samples and preparation

Plankton samples from the North- and the South Atlantic Ocean were investigated. The North Atlantic sample (POS 334, stat. 4 MSN K7) material derives from 0–100 m,

100–200 m, 200–300 m, 300–500 m and 500–700 m water depth and the South Atlantic sample (AMT 18, CTD 89) consists of three samples from 0 m, 48 m and 96 m water depth. Both sample series were preserved with formalin and hexamine after collection to avoid bacterial growth and to buffer the carbonate system.

The target prepared TEM samples were obtained by FIB sectioning. Radiation damage under ion bombardment can easily occur (Mayer *et al.*, 2007). In order to protect and preserve the structure of the coccolith, a thin (50 nm) carbon layer was deposited by electron beam induced deposition (EBID) at 3 kV. A further, thicker protection layer was deposited with successive ion beam induced deposition (IBID) with a beam current of 300 pA at 30 kV. Here carbon was used as well. The resulting layer thickness of around 1.0 μm was found to be thick enough to protect *E. huxleyi* from radiation damage during the following lamella cutting process. Additional plan view samples of *E. huxleyi* were prepared from the North Atlantic sample series. The sample was dropped on a copper TEM grid with a holey carbon film. Afterwards the samples were thinned according to the procedure developed by Wilbur & Watabe (1963) and Watabe (1967). Instead of using hydrochloric acid (HCl) we performed thinning with distilled $H_2O$ for several hours. This has the advantage of being gentler than the HCl treatment, so the fine structure and the full assembly of the coccolith stay intact.

### Instrumentation

For SEM imaging and FIB sectioning a Zeiss NVision40 FIB microscope was used, which combines the technologies of a GEMINI electron column, with a focused ion beam (zeta FIB column - operated at 30 kV) and single-injector multi-channel gas injection system (GIS). Secondary electron images were acquired at a low acceleration voltage of 2.5 kV. For TEM investigations we used a FEI Titan 80–300 kV field emission scanning (S)/TEM equipped with an energy-dispersive X-ray spectrometer and a Gatan imaging filter. The measurements were performed at 80 kV. The crystallographic orientations within the coccolith were investigated by bright-field imaging, selected-area electron diffraction, nano-probe diffraction and high-resolution imaging. For the selected-area electron diffraction an aperture of approximately 150 nm was used and for the nano-probe experiments a beam diameter of around 6 nm was applied.

## Results

A secondary-electron image of a complete coccosphere of *E. huxleyi* is given in Fig. 1a. To obtain crystallographic information of the R- and V-unit (Young *et al.*, 1992) (model given in Fig. 1d), cross-section samples are required. The V-unit can only be seen in the cross-section view as the R-unit overgrows the V-unit during the crystal growth phase of the coccolith formation (Young *et al.*, 1992).

The FIB sectioning allowed us to analyze the specimen in the SEM mode and to get a cross-section of the area of interest. Figure 1b shows a secondary-electron image of a cross-section through a complete coccosphere, where several (minimum 4) concentric layers of coccoliths can be observed. The coccoliths are relatively densely packed. The cell cavity, where the living cell resides, has a diameter of around 4 μm and is clearly visible. The concentric coccolith skeleton has a thickness of about 2.5 μm.

For the TEM investigations we used six different cross-section lamellae through single coccoliths. The bright-field TEM image of Fig. 1c shows as example one of those cross-sections. The 0–100 m and 100–200 m sample from the North Atlantic and the three samples from the South Atlantic series (0 m, 48 m 96 m) were used for this preparation method. We found the optimal thickness of the TEM lamellae to be between 70 nm and 90 nm. With thicker lamellae problems due to double diffraction during electron diffraction experiments occurred, while thinner samples were easily damaged by the electron beam bombardment.

First TEM measurements were performed at 300 kV and a low electron dose, meaning that a low number of electrons hit the sample per $m^2$. Our experiments using these parameters indicate that the calcite shell of the coccoliths is very sensitive to beam bombardment, especially during high-resolution imaging and selected-area electron diffraction experiments. After a few seconds of 300 kV electron bombardment the calcite transformed to a polycrystalline material with *d*-spacings indicating the formation of calcium oxide (CaO). Since the kind of beam damage differs between 80 kV and 300 kV (Williams & Carter, 2009), the parameters for the TEM measurements were changed to an acceleration voltage of 80 kV and a low dose. All experiments shown were performed under these conditions. These conditions allowed high-resolution imaging and electron diffraction measurements, while the sample stayed intact. However, even under these conditions electron bombardment for more than three minutes transformed the calcite to calcium oxide.

At 80 kV and a low dose, diffraction patterns of different areas of the cross-section of coccolith segments of *E. huxleyi* were taken from six different TEM lamellae. The achieved diffraction patterns were indexed, the lattice orientation was calculated and the **c**-axis was projected into the corresponding bright-field image (Fig. 2). The rotation between image and diffraction pattern is compensated in the used FEI Titan TEM. Our experiments showed that the **c**-axes of the different elements (proximal-, distal- and central-area element) within the R-unit of *E. huxleyi* lie within the coccolith plane. For the R-unit the **b**-axis is perpendicular to the coccolith plane (Fig. 2e). A representative bright-field image of an R-unit area is given in Fig. 2a. In Fig. 2b the corresponding electron diffraction pattern of the encircled area in Fig. 2a is shown. The electron diffraction pattern taken from the area where the V-unit should occur (Fig. 2c) reveals that here the [001] direction is perpendicular to that of the R-unit (marked by the white arrow in Fig. 2d). This orientation was predicted by

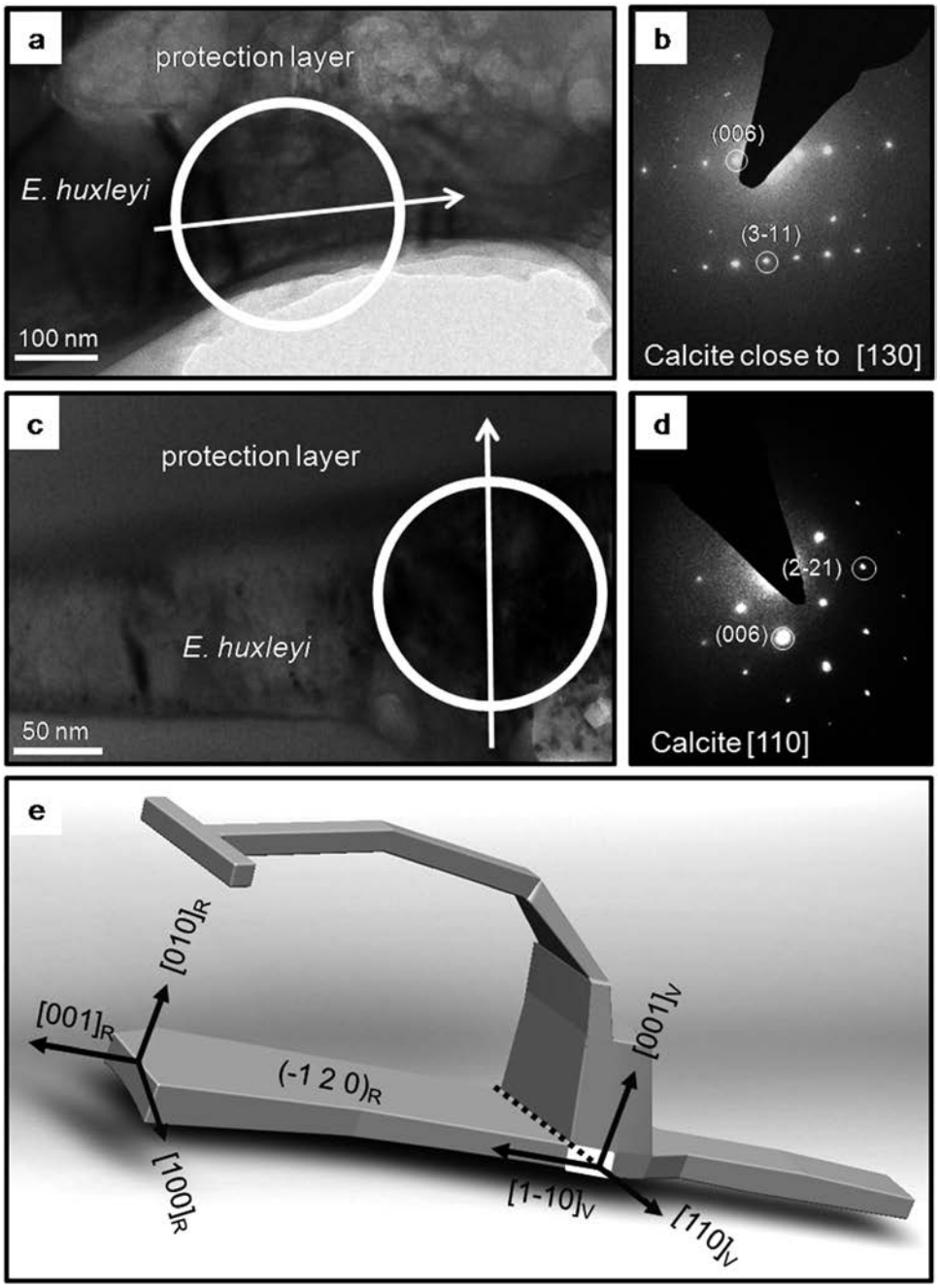


Fig. 2. V/R unit of *E. huxleyi* coccolith shield elements. a) Bright-field TEM image of the proximal shield element of *E. huxleyi*. The white arrow shows the projection of the crystallographic **c**-axis determined from the diffraction pattern given in b. The **b**-axis lies perpendicular to the coccolith plane and the **c**-axis is oriented parallel to the coccolith plane. The angle between the zone axis and the **b**-axis is approximately 14°. b) Electron diffraction pattern of the marked area (white circle in a). The diffraction pattern indicates calcite tilted close to the [130] zone axis. During the experiments the tilt angles were $\alpha = 11.6°$ and $\beta = 3.1°$. c) A bright-field TEM image of the V-unit of *E. huxleyi*. The V-unit [110] direction is in tangential direction of the coccolith ring and the **c**-axis (white arrow) direction is pointing perpendicular to the coccolith plane. d) Electron diffraction pattern of the marked area (white circle in c) indicating calcite tilted to the [110] zone axis. Compared to the diffraction pattern in b, the sample was tilted to $\alpha = 0.7°$ and $\beta = 4.6°$. e) Crystallographic orientation of the R- and the V-unit in a three-dimensional sketch of coccolith segment of *E. huxleyi*.

(Young *et al.*, 1992), based on analogy with other coccoliths. The analysis of our diffraction experiments revealed that the [110] direction of the V-unit is in tangential direction of the coccolith ring and its [1–10] direction is radial with respect to the coccolith ring (Fig. 2e).

The mesoscale crystallographic constitution of the *E. huxleyi* calcite was investigated by nano-probe electron diffraction experiments, as well as by bright-field and high-resolution imaging with the same parameters as given above. Due to the complex three-dimensional

structures of the coccolith segments (Fig. 3c), the FIB cross-section can pass through three different segments instead of one (see bright-field plan view image, Fig. 3). The visible elements (distal shield-, the proximal shield- and the central-area element), of one coccolith segment, are labeled as B. The white rectangle marked in Fig. 3b is a potential position for a FIB cross-section. This cross-section would pass through the distal shield element of the segment labeled as C, the proximal shield element of the segment labeled as B, and the central area element of the segment labeled as A. If the **c**-axis is expected to be precisely radial with respect to the ring, measurements using such a cross-section would show different crystal orientations for the elements, as they belong to differently oriented segments (A, B, C). To avoid these problems samples viewed perpendicular to the coccolith ring (plan view samples) were used in the experiments.

To investigate the orientation within one coccolith segment and to study the arrangement of the calcite crystals we performed nano-probe diffraction experiments on plan view samples. For these experiments the samples from the North Atlantic series taken from 200–300 m and 300–500 m were used. With this method a high spatial resolution (around 6 nm in our experiments) could be achieved. The measurements were started by tilting one area of the coccolith cross-section to a zone axis. Then these goniometer angles were kept while the whole element was investigated in the diffraction mode by translation of the sample holder. The nano-probe diffraction patterns obtained were overlain using a color code for the Kikuchi lines. If any crystallographic orientation variations occurred within one coccolith element, this procedure would enable us to detect this mosaic structure.

We studied seven distal- and proximal shield elements using two different plan view samples. We took 21 nano-probe diffraction patterns of the distal shield elements and 11 nano-probe diffraction patterns of the proximal shield elements. Within the distal shield element we only used the area, where the proximal shield element did not contribute to the diffraction pattern. Figure 4 shows the results of one diffraction experiment in the distal shield element (Fig. 4f). The Kikuchi lines in the nano-probe diffraction patterns (Fig. 4a–d) are marked by different colors. These patterns were overlain (Fig. 4e) and the overlain Kikuchi lines of

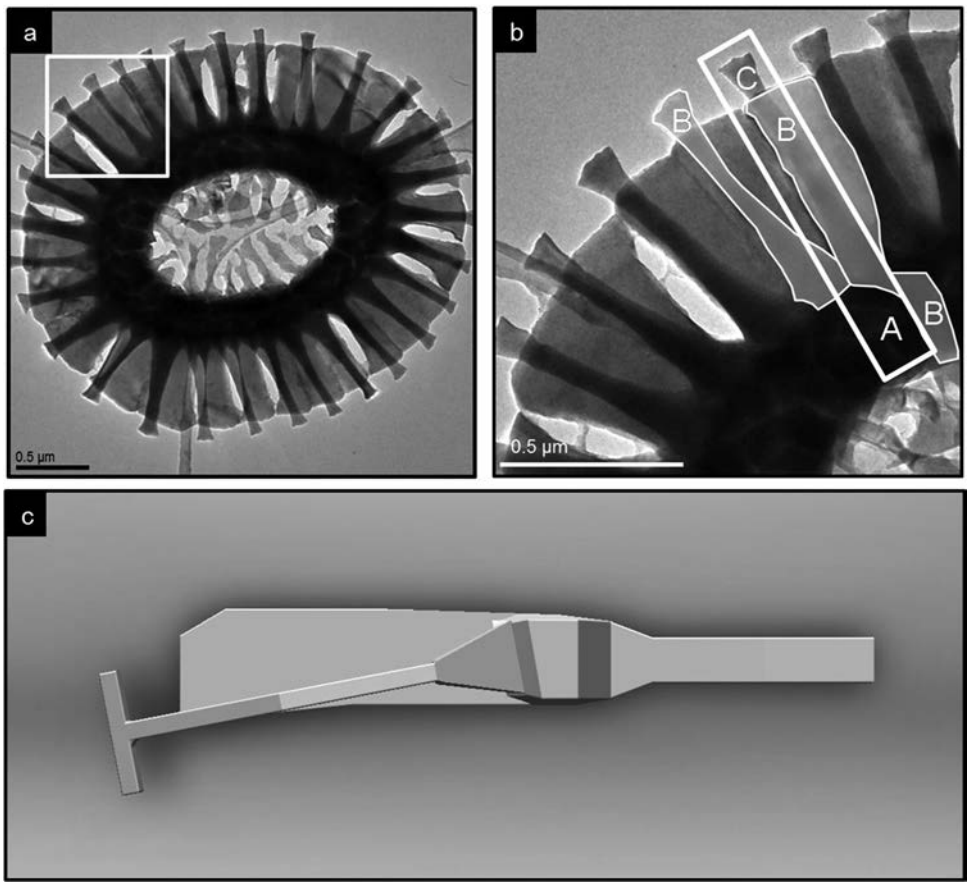


Fig. 3. Three-dimensional structure of *E. huxleyi* segments. a) Bright-field TEM image of an incomplete grown coccolith of *E. huxleyi*, in plan view. The white rectangle marks the area enlarged in b. b) Three visible elements composing one segment (distal shield element, proximal shield element and central-area element) are outlined by a thin white line and labeled by B. The white rectangle marks the position of a potential FIB-section cutting through the elements of three different coccolith segments (A, B, and C). Such a FIB lamella would contain the distal shield element of the coccolith segment C, the proximal shield element of the coccolith segment B, and the central-area element of the coccolith segment A. c) Three-dimensional model to illustrate the complex three-dimensional structure of a coccolith segment.

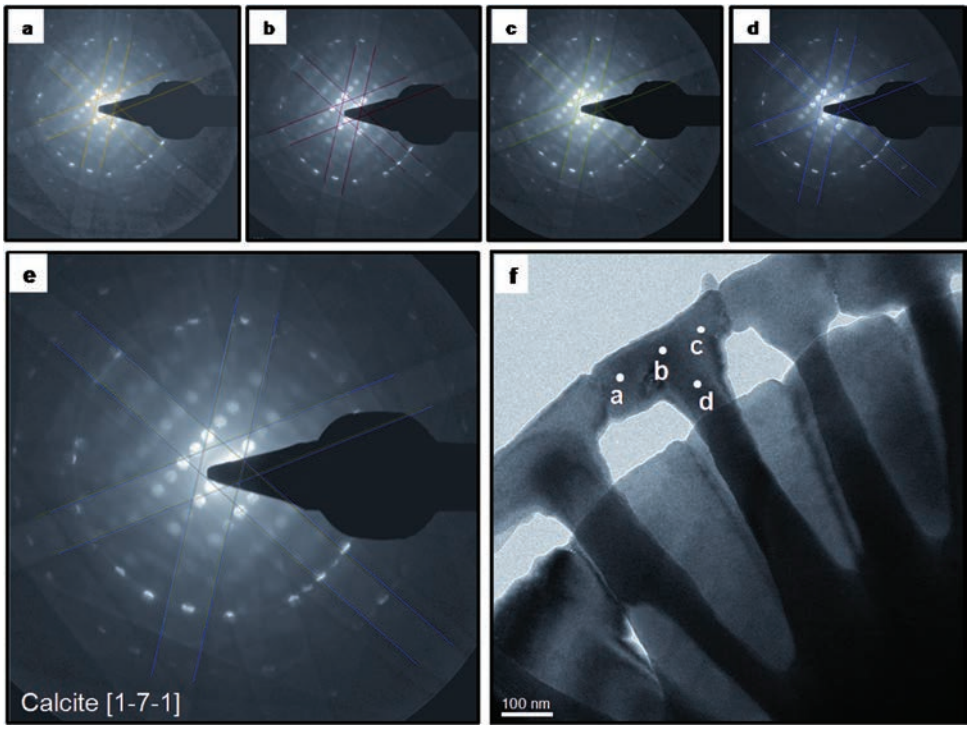


Fig. 4. Nano-probe diffraction within the distal shield element of *E. huxleyi*. a–d) Nano-probe electron diffraction patterns of the distal shield element of *E. huxleyi* marked in the bright-field image given in 4f. The Kikuchi lines are colored in yellow (4a), in red (4b), in green (4c) and in blue (4d). e) Overlain diffraction patterns a–d of the distal shield element. The Kikuchi lines show no evidence of relative misorientations between the patterns a–d within the experimental uncertainty of circa 1°. f) Bright-field image of a plan view sample with the position of the diffraction patterns (a–d) marked by white dots.

this area do not reveal tilting or rotation of the Kikuchi lines. An experimental uncertainty of 1° must be considered for this method (Williams & Carter, 2009). Accordingly the tip of the distal shield element of *E. huxleyi* has a coherent single-crystal-like lattice, as no indication of misorientations or a mosaic-like crystalline constitution within a precision of ± 1° was found.

The same result was obtained for the outer rim of the proximal shield element. In order to investigate if the distal- and the proximal shield element together form one single crystal additional nano-probe diffraction experiments with plan view samples were performed (Fig. 5). We tilted the distal shield element to a zone axis (Fig. 5a) and, while keeping the goniometer angles constant, acquired a diffraction pattern of the proximal shield element (Fig. 5b). The positions where the diffraction patterns were taken are marked in the bright-field image in Fig. 5c. These diffraction patterns were overlain (Fig. 5d). Two out of three Kikuchi pairs were found to be shifted with respect to each other. Using the calibrated camera constant we calculated from these shifts a relative tilt angle (Williams & Carter, 2009) of 4° ± 1° around the (101) plane normal direction. These observations are based on the investigation of three different pairs of distal- and proximal shield elements. Further investigations of the Kikuchi lines showed that these shifts start already within the middle of the distal shield element (white cross in Fig. 5c) with a tilt angle of approximately 1−2°.

We also investigated the change of lattice orientation between different coccolith segments (Fig. 6). The bright-field image in Fig. 6a shows the entire *E. huxleyi* coccolith with the area where we measured the rotation between three different segments marked by a gray square. The location of the diffraction patterns on the three segments are given in the bright-field image in Fig. 6b. In Fig. 6c the nano-probe diffraction patterns of the distal shield elements of segment 1 and segment 2 are overlaid. Using the Kikuchi lines of both segments (white for segment 1 and black for segment 2), we found that the segments are rotated by 8° ± 1° relative to each other around the direction normal to the coccolith ring. The same experiment was performed with the nano-probe diffraction pattern of segment 2 (Kikuchi lines given in black) and segment 3 (Kikuchi lines given in white), where we obtained a rotation of 7° ± 1° between the segments (Fig. 6d). This is in accordance to the value that we obtain geometrically from the elliptical shape of the coccolith.

For detailed analyses of the coccolith segments such as distal shield-, proximal shield- and central area element high-resolution imaging was performed. Within the elements, the high-resolution images showed no evidence for a nano-mosaic or for intra-crystalline organic matrix. Figure 7b is an example of a high-resolution image taken of an area of the distal shield element, which is indicated in the bright-field image shown in Fig. 7a.

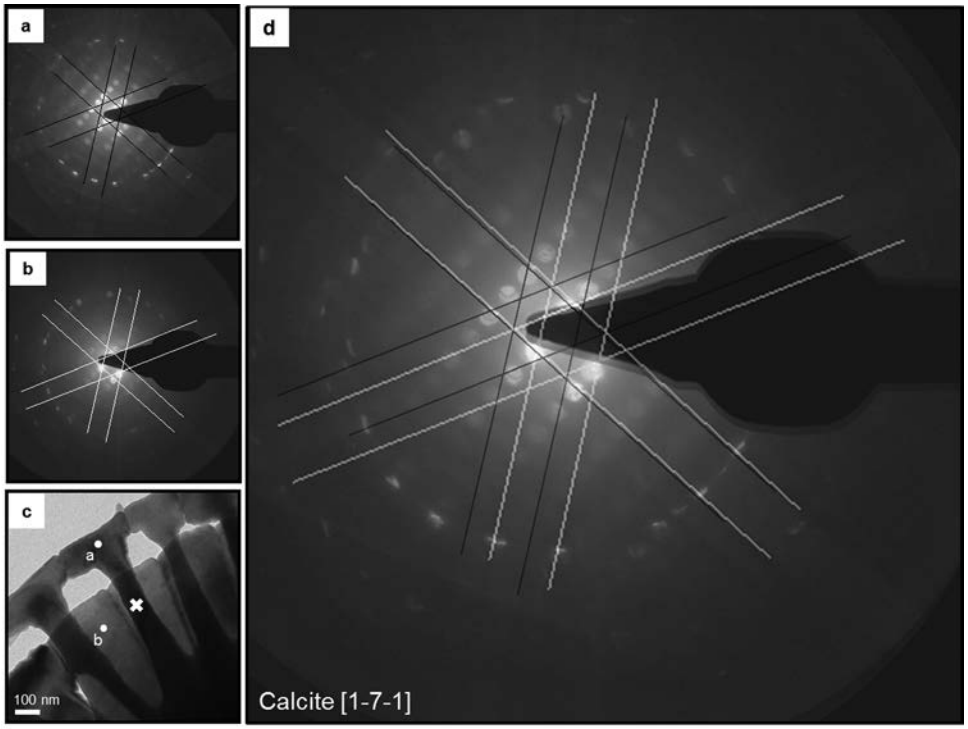


Fig. 5. Nano-probe diffraction of the distal- and the proximal shield element of *E. huxleyi*. a) Nano-probe electron diffraction pattern of the distal shield element of *E. huxleyi* marked in the bright-field image given in 5c. The Kikuchi lines are marked by black lines. b) Nano-probe diffraction pattern of the proximal shield element marked in the image given in 5c. The Kikuchi lines are marked by white lines. c) Bright-field image of a plan view sample with the position of the diffraction patterns 5a und 5b marked. The white dots mark the location where the nanoprobe electron diffraction patterns were taken and the white cross shows the area where the shift in the Kikuchi lines starts. d) Overlaid diffraction patterns of the distal and the proximal shield elements. The overlaid Kikuchi lines show a parallel translation for two pairs of Kikuchi lines. This is caused by tilting of $4^\circ \pm 1^\circ$ around the (101) plane normal.

## Discussion

Investigations of coccoliths by TEM were done in previous studies (Watabe, 1967; Mann & Sparks, 1988; Didymus *et al.*, 1994; Davis *et al.*, 1995; Saruwatari *et al.*, 2008b), which applied different methods to prepare electron-transparent TEM samples. Several groups washed, centrifuged and dispersed the culture samples on TEM grids and finally used etching to obtain sufficiently thin samples (Wilbur & Watabe, 1963; Watabe, 1967). This sample preparation method could produce only plan view TEM samples. Another preparation method was to sonicate the coccolith suspension for one minute and disperse this suspension on a TEM grid (Mann & Sparks, 1988; Didymus *et al.*, 1994; Davis *et al.*, 1995). This method allowed to obtain plan view and cross-section samples, which represented randomly-oriented cuts through coccolith segments. Wilbur & Watabe (1963) and Watabe (1967) used a preparation method to gain only cross-section samples: dried cultured samples were embedded in Vestopal H and cut with a diamond knife. However, the coccolith rings disintegrated such that the sample consisted of a random distribution of coccolith segments so that a well-defined cross-section could not be obtained. Our results show that the preparation method using FIB sectioning is able to produce site specific, oriented beam-transparent cross-sections through coccoliths.

Previous studies revealed that crystals of the V- unit could be found in very early growth stages in proto-coccolith rings (Young *et al.*, 1992). These crystals were reported to have an average size of 30–60 nm (Young *et al.*, 1992). Due to their size and the fact that they will be overgrown by R-crystals in later stages of development it was not possible to determine the crystallographic orientation of the V-units by light microscopy or electron diffraction (Young *et al.*, 1992) so far. With the target-preparation method we applied, we were able to detect the overgrown V-unit in fully grown coccolith segments of *E. huxleyi*. With the help of selected-area electron diffraction and bright-field imaging in TEM we found the [001] direction of the R-unit parallel and the [010] direction perpendicular to the coccolith plane. The V-unit [001] direction is perpendicular while the [1–10] direction is parallel to the coccolith plane oriented. Our electron microscopy study thus confirms the V- and R-model of the **c**-axis orientation obtained by light microscopy of Young *et al.* (1992) for *E. huxleyi* and it complements the full crystallographic orientation.

Mann & Sparks (1988) described in their study that the crystallographic **c**-axis of the proximal shield element is

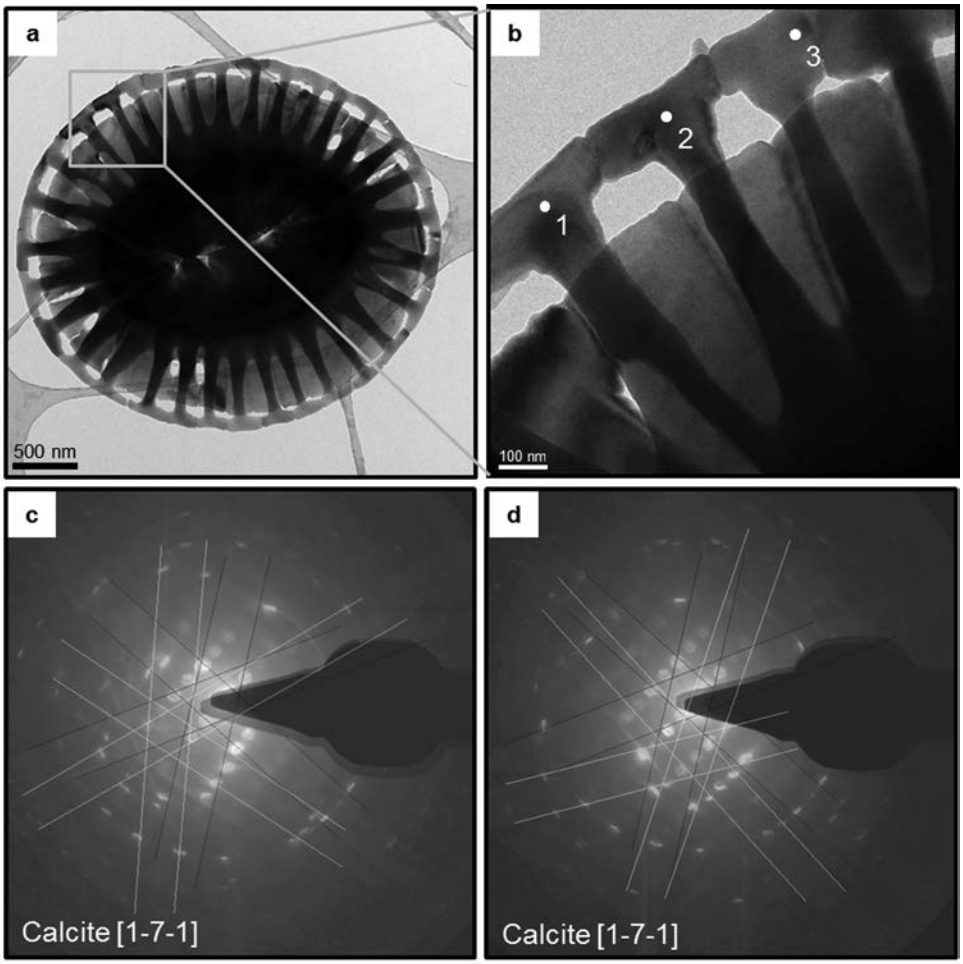


Fig. 6. Diffraction experiments to determine the angle between different segments of *E. huxleyi*. a) Bright-field image of *E. huxleyi*, with the position of the measurement marked by the gray square. b) Bright-field image with the position of the nano-probe diffraction pattern 1, 2 and 3 marked by white dots. c) Overlain diffraction patterns of position 1 (Kikuchi lines are marked in white) and 2 (Kikuchi pattern marked in black). The Kikuchi lines indicate a rotation of $8^\circ \pm 1^\circ$ between these segments around the direction normal to the coccolith ring. d) Overlain diffraction patterns of position 2 (Kikuchi lines are marked in black) and 3 (Kikuchi pattern marked in white). The Kikuchi lines indicate a rotation of $7^\circ \pm 1^\circ$ between these segments around the direction normal to the coccolith ring.

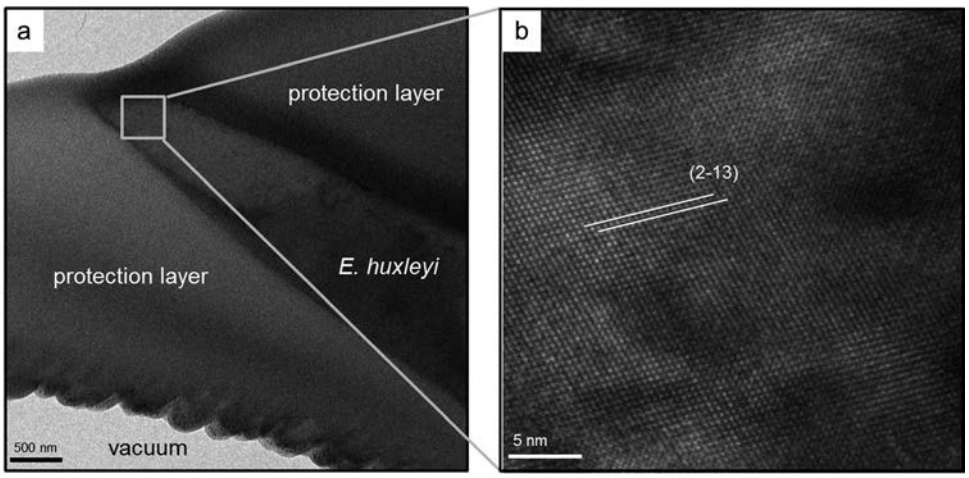


Fig. 7. High-resolution image of *E. huxleyi*. a) Bright-field TEM image showing the area for high-resolution imaging marked by the gray square. The protection layer is the carbon coating applied before FIB sectioning. b) The high-resolution TEM image of the coccolith element contains no crystal boundaries. The differences in contrast are due to the bending of the element.

parallel to the coccolith plane and the **b**-axis is perpendicular to the coccolith plane. Our electron diffraction patterns taken from isolated shield elements confirmed the single-crystal nature and the absence of a mosaic spread for both the proximal- as well as the distal shield element of *E. huxleyi*. However, in 1988 the mosaic-like assembly of biomaterial crystals was not known. So in this study the possibility that the coccolith calcite consists of a mosaic-like assembly was considered during the diffraction experiments.

Modern high-resolution studies of carbonate materials constituting the shells, spines, and teeth of marine organisms such as brachiopods, sea urchins, corals and mollusks showed that their carbonate crystals have a mosaic-like crystalline constitution (Neff, 1972; Feng *et al.*, 2000; Weiss *et al.*, 2002; Schmahl *et al.*, 2008; Vielzeuf *et al.*, 2010; Benzerara *et al.*, 2011; Seto *et al.*, 2012). Therefore we aimed to test if a mosaic-like crystalline structure is present in the calcite shell of *E. huxleyi*. Other studies (Mann & Sparks, 1988) had used selected-area electron diffraction, where the size of the illuminated area is determined by the selected-area diffraction aperture, typically 150 nm in diameter. In our study we performed experiments using nano-probe electron diffraction and Kikuchi lines, where tilting angles $\geq 1^\circ$ can be detected at high spatial resolution of around 6 nm. This method revealed no misorientations within the tip of the distal- and proximal shield element of *E. huxleyi* but we found a clear shift of the Kikuchi lines starting from the middle of the distal shield element leading to a crystallographic misorientation of $4^\circ \pm 1^\circ$ around the (101) plane normal direction. This is necessary to obtain the spherical shape of the coccosphere. In principle, different scenarios can account for this. First, the upper and lower shield element might be separated by a small angle tilt grain boundary. In that case, we would expect an abrupt change in the orientation visible in a clearly resolvable shift of the Kikuchi lines. Experimentally, we do not observe an abrupt change but instead we measure a continuous change in orientation when taking nano-probe diffraction pattern along the upper shield elements towards the central element. Second, the tilt could be obtained by geometrically necessary dislocations and we estimated that they should have a distance of around 7 nm to lead to an angle of 4°. These dislocations could be edge, screw or of mixed type. We did not observe strain fields associated with such dislocations; however, they could be invisible in the viewing directions used. Furthermore, the associated lattice distortion might be below the resolution limit of our microscope. A third possible explanation would be that the element is elastically bent due to a chemical gradient leading to a change in lattice parameters from top to bottom, due to stresses from the surrounding organic and/or due support by the surrounding organic or due to gravitational forces. This would lead to a continuous orientation change. However, assuming a Young's modulus of 70 GPa (Merkel *et al.*, 2009) for the shield elements, a stress (load per area) of around 4.6 GPa would be required to induce the 4° distortion mechanically. This essentially excludes mechanical stress as the origin of the misorientation, and since there is no evidence for a chemical gradient, dislocations seem to be the most likely explanation.

A single coccolith is shaped like a flat domed bowl, which is necessary to create the spherical coccosphere by an assembly of these bowls. The relative misorientation between the proximal- and the distal shield elements of *E. huxleyi* serves to obtain the flat domed character of the coccoliths.

The different segments of the coccolith ring are also rotated with respect to each other around the normal of the coccolith ring, in order to form the circumference of the ellipsoidal ring. For the segments which we measured the angle is in the order of $7–8^\circ \pm 1^\circ$. These values fit nicely with results of former studies using Kikuchi lines in TEM (Saruwatari *et al.*, 2008b). In the study of Saruwatari *et al.* (2008b) for each shield element one Kikuchi pattern was taken. Furthermore, they did not use several electron patterns within one shield element to investigate orientation changes.

Multi-cellular calcifiers, for which a mosaic like crystalline constitution of the carbonate crystals has been demonstrated (Neff, 1972; Weiss *et al.*, 2002; Aizenberg *et al.*, 2005; Griesshaber *et al.*, 2007; Jacob *et al.*, 2008; Benzerara *et al.*, 2011; Addadi *et al.*, 2012; Schmahl *et al.*, 2012) are formed in an extracellular process, where vesicles containing amorphous calcium carbonate are exocytosed and attach to the carbonate shell, spines, or teeth, where they crystallize with a slight misorientation to form a crystal with a mosaic-spread (Beniash *et al.*, 1997). In contrast the whole coccolith ring is produced in a vesicle inside the cell (Young & Henriksen, 2003). So far our high-resolution imaging gave no evidence for organic layers within one crystal unit, nor of any nanomosaicity. If the tilt of 4° between the distal- and the proximal shield element is caused by a chemical gradient, gravitational forces and/or by support of the surrounding organic, the coccoliths would differ from the multi-cellular marine calcifiers.

## Conclusion

In this study it has been shown that FIB sectioning of coccoliths can be used to gain pristine site specific cross-sections of the coccoliths of *E. huxleyi*. The described methods allowed to image and analyze the orientation of the overgrown V-unit. The analysis revealed that the [110] direction of the V-unit is in tangential direction of the coccolith ring and the [1–10] direction is radial with respect to the coccolith ring.

Our nanoprobe electron diffraction experiments with a precision of 1° reveal that the distal- and the proximal element of the R-unit show a relative tilt of $4^\circ \pm 1^\circ$ around the (101) plane normal direction. This misorientation starts already within the middle of the distal shield element. This tilt within and between the shield elements serves to obtain the flat domed character of the coccoliths, which is necessary to form a coccosphere. The high-resolution TEM

images do not show evidence of a mosaic-like assembly of the calcite crystals of the shield elements that build up the coccoliths of *E. huxleyi*.

For the future applying the techniques developed here to other coccoliths has great potential to elucidate the structure of coccolith species which are too small to study with optical microscopy and SEM. Hence we are confident that these techniques can significantly advance our knowledge of the range of biomineralisation patterns in coccoliths and the degree to which variation in such patterns is responsible for the extraordinary diversity in coccolith forms.

**Acknowledgement:** Special thanks go to Markus Döblinger and Steffen Schmidt for their advice and support at the microscope. We are indebted to Teresa Dennenwaldt LMU Munich and Klemens Kelm, DLR Cologne, for critically reviewing the manuscript. Alexander Müller assisted in this project. The authors are thankful for the three dimensional coccolith model drawn by Stefan Männl. The work is supported by the German Science Foundation [DFG, Grant Nr. SCHM 930/15-1]. R. H. is grateful for a stipendium by the Bayerische Eliteförderung (BayEFG).

## References

Addadi, L., Vidavsky, N., Weiner, S. (2012): Transient precursor amorphous phases in biomineralization in the footsteps of Heinz A. Lowenstam. *Z. Kristallogr.*, **227**, 711–717.

Aizenberg, J., Weaver, J.C., Thanawala, M.S., Sundar, V.C., Morse, D.E., Fratzl, P. (2005): Skeleton of *Euplectella sp.*: structural hierarchy from the nanoscale to the macroscale. *Science*, **309**, 275–278.

Beniash, E., Aizenberg, J., Addadi, L., Weiner, S. (1997): Amorphous calcium carbonate transforms into calcite during sea urchin larval spicule growth. *Proc. R. Soc. Lond. B.*, **264**, 461–465.

Benzerara, K., Menguy, N., Obst, M., Stolarski, J., Mazur, M., Tylisczak, T., Brown, G.E., Jr, Meibom, A. (2011): Study of the crystallographic architecture of corals at the nanoscale by scanning transmission X-ray microscopy and transmission electron microscopy. *Ultramicroscopy*, **111**, 1268–1275.

Davis, S.A., Young, J.R., Mann, S. (1995): Electron Microscopy studies of shield elements of *Emiliania huxleyi* Coccoliths. *Bot. Mar.*, **38**, 493–497.

Didymus, J.M., Young, J.R., Mann, S. (1994): Construction and Morphogenesis of the Chiral Ultrastructure of Coccoliths from the Marine Alga *Emiliania huxleyi*. *Proc. R. Soc. Lond. B.*, **258**, 237–245.

Feng, Q.L., Cui, F.Z., Pu, G., Wang, R.Z., Li, H.D. (2000): Crystal orientation, toughening mechanisms and a mimic of nacre. *Mat. Sci. Eng. C.*, **11**, 19–25.

Goetz, A.J., Griesshaber, E., Neuser, R.D., Lüter, C., Hühner, M., Harper, E., Schmahl, W.W. (2009): Calcite morphology, texture and hardness in the distinct layers of rhynchonelliform brachiopod shells. *Eur. J. Mineral.*, **21**, 303–315.

Griesshaber, E., Schmahl, W.W., Neuser, R., Pettke, T., Blum, M., Mutterlose, J., Brand, U. (2007): Crystallographic texture and microstructure of terebratulide brachiopod shell calcite: An optimized materials design with hierarchical architecture. *Am. Mineral.*, **92**, 722–734.

Honjo, S. (1976): Coccoliths: production, transportation and sedimentation. *Mar. Micropaleontol.*, **1**, 65–79.

Jacob, D.E., Soldati, A.L., Wirth, R., Huth, J., Wehrmeister, U., Hofmeister, W. (2008): Nanostructure, composition and mechanisms of bivalve shell growth. *Geochim. Cosmochim. Acta.*, **72**, 5401–5415.

Mann, S. & Sparks, N.H.C. (1988): Single Crystalline Nature of Coccolith Elements of the Marine Alga *Emiliania huxleyi* as Determined by Electron Diffraction and High-Resolution Transmission. *Proc. R. Soc. Lond. B.*, **234**, 441–453.

Mayer, J., Giannuzzi, L.A., Kamino, T., Michael, J. (2007): TEM sample preparation and FIB-induced damage. *MRS Bull.*, **32**, 400–407.

McIntyre, A. (1967): Coccoliths as paleoclimatic indicators of Pleistocene glaciation. *Science*, **158**, 1314–1317.

Merkel, C., Deuschle, J., Griesshaber, E., Enders, S., Steinhauser, E., Hochleitner, R., Schmahl, W.W. (2009): Mechanical properties of modern calcite- (*Mergerlia truncata*) and phosphate-shelled brachiopods (*Discradisca stella* and *Lingula anatina*) determined by nanoindentation. *J. Struc. Biol.*, **168**, 396–408.

Neff, J.M. (1972): Ultrastructure of the outer epithelium of the mantle in the clam *Mercenaria mercenaria* in relation to calcification of the shell. *Tissue & Cell*, **4**, 591–600.

Riley, J. Chester, J.P. & Chester, R. (eds) (1976): Treatise on Chemical Oceanography. Academic Press, London, 543 p.

Rousseau, M., Lopez, E., Stempflé, P., Brendlé, M., Franke, L., Guette, A., Naslain, R., Bourrat, X. (2005): Multiscale structure of sheet nacre. *Biomaterials*, **26**, 6254–6262.

Saruwatari, K., Ozaki, N., Nagasawa, H., Kogure, T. (2006): Crystallographic alignments in a coccolith (*Pleurochrysis carterae*) revealed by electron back-scattered diffraction (EBSD). *Am. Mineral*, **91**, 1937–1940.

Saruwatari, K., Ozaki, N., Nagasawa, H., Kogure, T. (2008a): Comparison of crystallographic orientations between living (*Emiliania huxleyi* and *Gephyrocapsa oceanica*) and fossil (*Watznaueria barnesiae*) coccoliths using electron microscopes. *Am. Mineral.*, **93**, 1670–1677.

Saruwatari, K., Akai, J., Fukumori, Y., Ozaki, N., Nagasawa, H., Kogure, T. (2008b): Crystal orientation analyses of biominerals using Kikuchi patterns in TEM. *J. Miner. Petrol. Sci.*, **103**, 16–22.

Sato, T., Kameo, K., Takayama, T. (1991): Coccolith biostratigraphy of the Arabian Sea. *Proc. ODP, Sci. Results*, **117**, 37–54.

Schmahl, W.W., Griesshaber, E., Merkel, C., Kelm, K., Deuschle, J., Neuser, R.D., Goetz, A., Sehrbrock, A., Mader, W. (2008): Hierarchical fibre composite structure and micromechanical properties of phosphatic and calcitic brachiopod shell biomaterials – an overview. *Mineral. Mag.*, **72**, 541–562.

Schmahl, W.W., Griesshaber, E., Kelm, K., Ball, A., Goetz, A., Xu, D., Kreitmeier, L., Jordan, G. (2012): Towards systematics of calcite biocrystals: insight from the inside. *Z. Kristallogr.*, **227**, 604–611.

Seto, J., Ma, Y., Davis, S.A., Meldrum, F., Gourrier, A., Kim, Y., Schilde, U., Sztucki, M., Burghammer, M., Maltsev, S., Jäger, C., Cölfen, M. (2012): Structure-property relationships of a biological mesocrystal in the adult sea urchin spine. *Proc. Natl. Acad. Sci.*, **109**, 7126–7126.

Song, R.-Q. & Cölfen, H. (2010): Mesocrystals–ordered nanoparticle superstructures. *Adv. Mater.*, **21**, 1–30.

Stanley, S.M. (1999): Earth System History. W.H. Freeman and Company, New York, p. 537.

Vielzeuf, D., Floquet, N., Chatain, D., Bonnete, F., Ferry, D., Garrabou, J., Stolper, E.M. (2010): Multilevel modular mesocrystalline organization in red coral. *Am. Mineral.*, **95**, 242–248.

Watabe, N. (1967): Crystallographic analysis of the coccolith of *Coccolithus huxleyi*. *Calc. Tiss. Res.*, **1**, 114–121.

Weiss, I.M., Tuross, N., Addadi, L., Weiner, S. (2002): Mollusc larval shell formation: amorphous calcium carbonate is a precursor phase for aragonite. *J. Exp.Zool.*, **293**, 478–491.

Wilbur, K.M. & Watabe, N. (1963): Experimental studies on calcification in molluscs and the alga *Cocolithus huxleyi*. *Ann. N. Y. Acad. Sci.*, **109**, 82–112.

Williams, D.R. & Carter, B.C. (2009): Transmission Electron Microscopy. A Textbook for Material Sciences. Springer-Verlag, New York, p. 779.

Winter, A. & Siesser, G.W. (eds) (1994): Coccolithophores. University Press, Cambridge, p. 242.

Young, J.R. & Henriksen, K. (2003): Biomineralization Within Vesicles: The Calcite of Coccoliths. *Reviews Min. Geochem.*, **54**, 189–215.

Young, J.R., Didymus, J.M., Bown, P.R., Prins, B., Mann, S. (1992): Crystal assembly and phylogenetic evolution in heterococcoliths. *Nature*, **356**, 516–518.

Young, J.R., Bergen, J.A., Bown, P.R., Burnett, J.A., Fiorentino, A., Jordan, R.W., Kleijne, A., van Niel, B.E., Romein, A.J.T., von Salts, K. (1997): Guidelines for coccolith and calcareous nanofossil terminology. *Palaeontology*, **40**, 875–912.

Young, J.R., Davis, S.A., Bown, P.R., Mann, S. (1999): Coccolith ultrastructure and biomineralisation. *J. Struct. Biol.*, **126**, 195–215.

Young, J.R., Geisen, M., Cros, L., Kleijne, A., Sprengel, C., Probert, I., Østergaard, J. (2003): A guide to extant coccolithophore taxonomy. *J. Nanoplankton Res.*, 1–132.

*Received 23 September 2013*
*Modified version received 15 November 2013*
*Accepted 6 December 2013*